

COLLAPSE MODES OF CONCRETE REINFORCED SQUARE BRIDGE PIERS UNDER VEHICLE COLLISION

XIUNENG ZHOU

School of Rail Transportation, Soochow University, Suzhou, China

ZHONGYOU XIE

School of Architectural Engineering, Tongling University, Tongling, China

e-mail: zhyxie@126.com

ZHIXIAN ZHAO, CHENG LI

School of Rail Transportation, Soochow University, Suzhou, China

Corresponding author Cheng Li, e-mail: licheng@suda.edu.cn

In the field of engineering protection, there is a structural disaster named heavy vehicles impacting column structures. When a heavy truck collides with a reinforced concrete (RC) column at a high velocity, a large impact force generated makes perhaps the column fail and even collapse. Therefore, it is necessary to study the dynamic characteristics during such a disaster, which can provide some reference for structural design, optimization and protection. The RC column impacted by a vehicle could be simplified as a beam fixed at the bottom loaded by a concentrated force, whose deformation is controlled by shearing and bending. In the present work, the ultimate static forces corresponding to shearing and bending collapse are proposed based on theoretical analyses. The model validation is performed using the finite element approach and the theoretical analytical results are in good agreement with the finite element simulation results, which validates the present analytical model. Three cases are simulated by utilizing finite element code ABAQUS, which reveals that the approximate plateau collapse force keeps a long stage beyond the peak failure one. In addition, three collapse modes are observed based on the static force and deformation analysis, validating the present framework which can be used for routine pier design. The work can be extended to estimate collapse modes of building columns under a vehicle collision.

Keywords: RC square pier, collapse mode, vehicle collision, numerical simulation

1. Introduction

As transport infrastructure develops rapidly in recent years, the vehicle collision with bridge piers events increase sharply (El-Tawil *et al.*, 2005; Tsang and Lam, 2008). Vehicular collision with piers would bring about the whole bridge or its part collapsing and the loss of human life (Harik *et al.*, 1990; Sharma *et al.*, 2012). According to the statistics, from 1980 to 2012, 15% of bridge collapses in the United States was caused by vehicle collisions, ranking the third of bridge collapse reasons (Abdelkarim and ElGawady, 2016). Suter (2005) found that the amount of vehicle collisions with bridge piers noticeably increases in European countries during past decades.

In the past few decades, theories and methods of structural vibration and impact dynamics involved in the collision have been extensively studied (Auyeung *et al.*, 2019; Chehaibi *et al.*, 2019; Ding *et al.*, 2014; Gholipour *et al.*, 2018; Hu *et al.*, 2020, 2021; Lim and Liew, 1994, 1995; Lim *et al.*, 1998; Warzecha and Michalczyk, 2020; Yan *et al.*, 2019a,b; Yang *et al.*, 2018), which provide the necessary theoretical basis and premise for the actual engineering research of heavy vehicles impacting piers. Due to the increasing number of accidents of vehicles impacting

with piers, a number of related investigations were conducted in the recent years. For examples, El-Tawil *et al.* (2005) performed finite element simulations of collisions between trucks and bridge piers and concluded that current American Association of State Highway and Transportation Officials (AASHTO) design provisions could be unconservative. In terms of experimental results of the full-size vehicle-pier collision, Buth *et al.* (2011) suggested a higher impact force of 2669 kN as the design standard. Fujikake *et al.* (2009) developed an analytical model to predict the maximum midspan deflection and maximum impact load validated by experimental results. Chen *et al.* (2016a) proposed a reduced model to simulate the vehicle collision with piers, which reasonably represented the behavior of a set of coupled vehicle-bridge systems.

The existing research indicated that RC piers experience three collapse modes including shear collapse, flexural collapse and flexure-shear collapse under a lateral collision. Abdelkarim and ElGawady (2017) proved that a bridge collapse was dominated by the shear collapse mode under the vehicle collision. The investigation of Zhou *et al.* (2017) revealed that bridge piers showed a flexure-shear collapse as vehicular impact energy was smaller, otherwise the shear collapse would occur. A recent study by Do *et al.* (2018) reported that piers had also experienced a punching shear collapse except for common collapse modes. The dynamic response and collapse modes of bridge piers under the vehicle collision have been considerably investigated, and most of them were conducted by numerical simulations (Abdelkarim and ElGawady, 2016; Chen *et al.*, 2016b; Tsang and Lam, 2008). Kostek and Aleksandrowicz (2020) performed reconstruction of a crash of a passenger car into a pillar using software V-SIM4 as compared with the corresponding crash test.

Though vehicle collision on piers is evidently dynamic in nature, the specifications of several countries, including the USA, China and UK, etc., recommend static analysis exempt from dynamic complexities (Joshi and Gupta, 2012). In this study, an analytical model for the discrimination of collapse modes of RC square piers under lateral static loading is developed based on the classical elastic theory and some previous investigation results. Three engineering cases are simulated using finite element code ABAQUS to verify the predicted solutions.

2. Analytical models

2.1. Maximum internal static forces

Generally, the bottom of the bridge piers is fixed with a foundation, while the top of those would be restrained by superstructures along the longitudinal direction of bridges. So, the pier under lateral loading could be reduced to a beam loaded by a concentrated force, fixed at the bottom end and simply-supported at the top end, see Fig. 1. Due to a small range of the contact region between the vehicle and pier along the pier axis, the impact load could be assumed as a concentrated one represented by F , which agrees with the Industry Standards of the People's Republic of China-General Specifications for Design of Highway Bridges and Culverts (ISPRC-DHBC, 2015) and the American Association of State Highway and Transportation Officials-Load and Resistance Factor Bridge Design Specifications (AASHTO-LRFD, 2012). The whole length of the pier and that of the loading point are denoted by H_0 and H , respectively. It is indicated that the axial force has little influence on transverse collision (Suter, 2005), so the axial force effect is neglected accordingly.

On the basis of classical elastic theory, the formulation of the maximum shear force would show the following form

$$F_s = F \left(1 - \frac{3H^2}{2H_0^2} + \frac{H^3}{2H_0^3} \right) \quad (2.1)$$

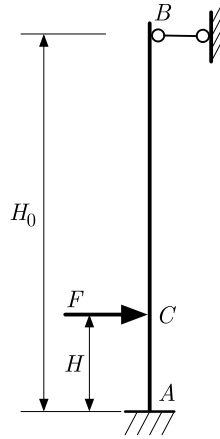


Fig. 1. The simplified beam model impacted by a concentrated load

and the moments at the bottom and loading sections could be calculated respectively by

$$M_A = \frac{F(2H_0^2 - 3H_0H + H^2)H}{2H_0^2} \quad M_C = \frac{F(3H_0^2H^2 - 4H_0H_0^3 + H^4)}{2H_0^3} \quad (2.2)$$

Let the following dimensionless parameters be as follows

$$\bar{H} = \frac{H}{H_0} \quad \bar{F}_s = \frac{F_s}{F} \quad \bar{M} = \frac{M}{FH_0} \quad (2.3)$$

Thus, the normalized shear force and moments become

$$\begin{aligned} \bar{F}_s &= 1 - \frac{3}{2}\bar{H}^2 + \frac{1}{2}\bar{H}^3 & \bar{M}_A &= \bar{H} - \frac{3}{2}\bar{H}^2 + \frac{1}{2}\bar{H}^3 \\ \bar{M}_C &= \frac{1}{2}(3\bar{H}^2 - 4\bar{H}^3 + \bar{H}^4) \end{aligned} \quad (2.4)$$

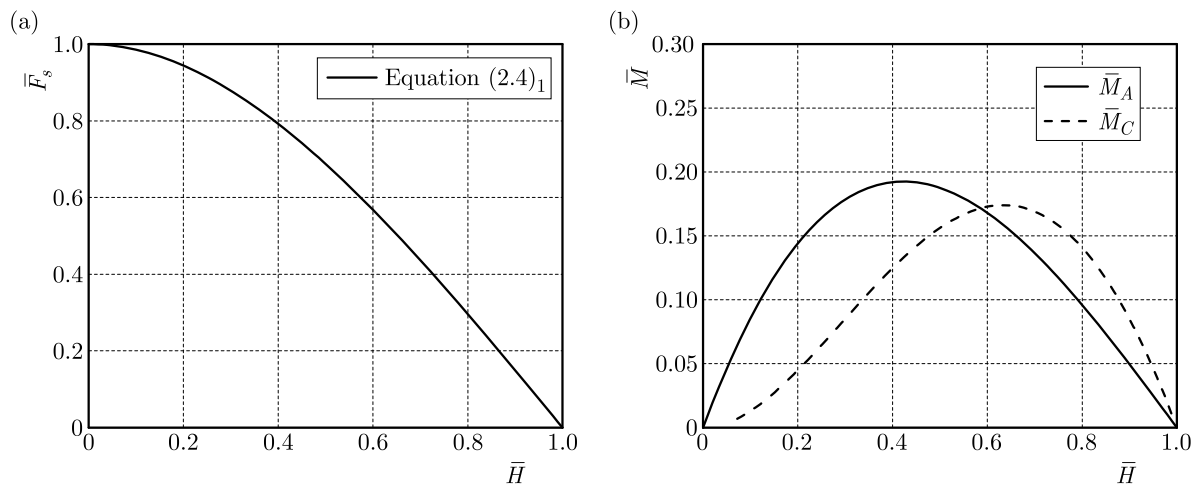


Fig. 2. Variation of (a) shear force and (b) moment with the height of loading spot

For the purpose of conveniently grasping the variation characteristic of the shear force and moments with the height of impact location, the above relationship is plotted in Figs. 2a and 2b. It can be found that the maximum shear force decreases with the height of the impact point, while the two moments both have a peak value. When the dimensionless height arrives at the critical value, i.e. 0.586, the moment at the bottom section is equal to that at the impact point

section. The height of the impact point is set as 1.2 m in ISPRC-DHBC and 1.5 m in AASHTO-LRFD, respectively. Considering the requirement of vehicles running underneath, the height of bridge piers generally reach more than 4.5 m, thereby the maximum moment would be that at the bottom section, i.e. M_A .

2.2. Load-carrying capacity of RC square columns

2.2.1. Shear resistance

Based on the 45 degree truss model according to AASHTO-LRFD, the total shear resistance of RC square section V_n consists of the nominal shear resistance of concrete V_c and transverse reinforcements V_s , i.e.

$$V_n = V_c + V_s \quad V_c = 149.3\sqrt{f'_c}b(b - 2a_s) \quad V_s = \frac{A_v f_{yv}(b - 2a_s)}{s} \quad (2.5)$$

where f'_c is the specified compressive strength of concrete at 28 days, A_v – area of transverse reinforcement within a distance s , f_{yv} – yield strength of transverse reinforcement, s – spacing of transverse reinforcement measured in the direction parallel to the longitudinal reinforcement. It is noted that in Eq. (2.5)₂ the unit of f'_c adopts MPa, while b and a_s is m. The unit of the resultant V_c is kN.

2.2.2. Flexural resistance

Considering the RC square section with side length b , the longitudinal reinforcements are uniformly distributed around the perimeter of the cross section, see Fig. 3a. To simplify the analysis, the decentralized longitudinal reinforcements are equivalent to a square steel tube with the same total cross-sectional area A_s and the distance between the center of longitudinal steels and sectional edge a_s , as illustrated in Fig. 3b.

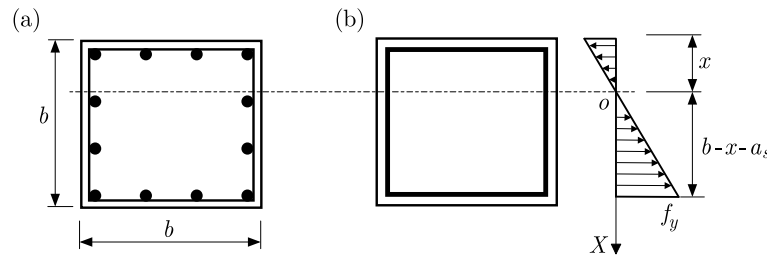


Fig. 3. Equivalent distribution of longitudinal reinforcements

The equivalent square steel tube is assumed to have an identical wall thickness t_s , which can be computed as

$$t_s = \frac{A_s}{4(b - 2a_s)} \quad a_s = c + d_v + \frac{1}{2}d_s \quad (2.6)$$

where the parameter c refers to the thickness of the concrete cover. d_v and d_s are the diameters of the longitudinal and transverse reinforcements, respectively.

Furthermore, two assumptions are proposed as follows:

- The section keeps always in a plane, and the strain distributes linearly along the direction perpendicular to the neutral axial;
- The longitudinal reinforcements in the tensile region up to ultimate tensile strain yield at first.

Therefore, the stress of the longitudinal steels σ_s and that of the concrete σ_c can be given respectively as below

$$\sigma_s = \frac{f_y}{b-x-a_s}X \quad \sigma_c = \frac{E_c}{E_s} \frac{f_y}{b-x-a_s}X \quad (2.7)$$

where x denotes the distance between the neutral axial and the compression concrete edge, which would be determined later. E_s and E_c are the elastic modulus of concrete and longitudinal steel, respectively.

Based on the force equilibrium relationship, the following equation would be obtained

$$\int_0^x b\sigma_c dX + \frac{f_y(b-2a_s)t_s}{b-x-a_s}(x-a_s) - f_y t_s(b-2a_s) - 2 \int_{-(x-a_s)}^{b-x-a_s} \sigma_s t_s dX = 0 \quad (2.8)$$

Using Eq. (2.6)₁ and (2.7), the above equilibrium equation would be reduced to

$$\frac{E_c}{E_s}bx^2 = A_s(b-2x) \quad (2.9)$$

Thus, the unknown x could be solved as

$$x = -\alpha b + \sqrt{\alpha b + \alpha^2 b^2} \quad (2.10)$$

where the parameter α is defined by

$$\alpha = \frac{A_s E_s}{A E_c} \quad (2.11)$$

Here $A_s = b^2$. Now, the ultimate moment M_n at the section can be computed by

$$M_n = \int_0^x b\sigma_c X dX + \frac{f_y t_s (x-a_s)^2}{b-x-a_s} + f_y t_s (b-2a_s)(b-x-a_s) + \int_{-(x-a_s)}^{b-x-a_s} 2\sigma_s t_s X dX \quad (2.12)$$

Using the previous relationship, the ultimate moment M_n would be reduced to

$$M_n = \frac{1}{12} A_s f_y \frac{2(b-2a_s)^2 + 4\alpha^{-1}b^{-1}x^3 + 3(b-2x)^2}{b-x-a_s} \quad (2.13)$$

2.3. The collapse static forces

Based on the general principle of strength design, when the actual internal force is smaller than the load resistance, the structures would not fail, i.e.

$$F_s \leq V_n \quad M_A \leq M_n \quad (2.14)$$

It is more convenient to compare the corresponding forces, and the static forces due to shear $[F_V]$ and flexural collapse $[F_M]$ are determined respectively by

$$[F_V] = \frac{V_n}{F_s} \quad [F_M] = \frac{M_n}{M_A H_0} \quad (2.15)$$

3. Finite element models and validation

As for the present research, namely on collapse modes of reinforced concrete square bridge piers subjected to a vehicle collision, there are generally several approaches to the examination such as theoretical modeling, numerical simulation and experiment. This paper focuses on a theoretical model in particular analytical models, but the theoretical model must be verified to make the results more credible. Considering the high cost of the full-scale impact experiment on vehicle collisions with bridge piers as well as the complexity of measurement technology of field tests, the theoretical model will be verified by numerical simulation. In fact, numerical simulations were widely used and verified in a number of previous studies (Chen *et al.*, 2016a,b; Kostek and Aleksandrowicz, 2020; Thilakarathna *et al.*, 2010). The finite element models have been established mainly based on the reference to previous strategies. To verify the proposed analytical models and solutions, the response of RC square piers with a height of 5.0 m subject to lateral loading is simulated using finite element code ABAQUS. Static displacement-load is applied and the average velocity approximates 1 m/s. The loading puncher perpendicular to one side of the square section is modeled as a rigid body, and the loading force is imparted at a height of 1.5 m above the ground (AASHTO-LRFD). The contact region is set 0.25 m (Thilakarathna *et al.*, (2010)) in height and side length b in width, respectively. The boundary conditions are identical with the above analytical model. Three cases are simulated, and the details of configuration of the piers are presented in Table 1.

Table 1. Configuration of the piers simulated in the FE models

Cases	Cross-section	Cover	Concrete grade	Longitudinal reinforcements	Transverse reinforcements
1	1.0 m×1.0 m	30 mm	C25	24Φ25 (HRB400)	Φ8(<i>HPB300</i>)@200
2				16Φ20 (HRB400)	Φ8(<i>HPB300</i>)200
3				16Φ20 (HRB400)	Φ12(<i>HPB300</i>)@100

The reinforcements are modeled as truss elements, and mechanical properties of those are provided in Table 2. The properties of the concrete material are referenced from ABAQUS Verification Guide (2010), where Young's modulus of the concrete is 26.48 GPa and Poisson's rate 0.167. Concrete damage plasticity model is utilized to describe concrete plasticity, and the needed parametric values are given in Table 3 and Table 4.

Table 2. Mechanical properties of the reinforcements

Category of reinforcements	Young's modulus [GPa]	Poisson's ratio [-]	Yield stress [MPa]
HRB400	200	0.3	400
HPB300	210	0.3	300

Table 3. Concrete damaged plasticity data

Dilation angle	Flow potential eccentricity	Biaxial/uniaxial compression plastic strain ratio	Invariant stress ratio	Viscosity
15°	0.1	1.16	0.6667	0.0

Table 4. Compression and tensile properties of concrete material

Compression			Tension		
Yield stress [MPa]	Inelastic strain	Damage	Yield stress [MPa]	Cracking strain	Damage
24.019	0	0	1.780	0	0
29.208	0.0004	0.1299	1.457	0.0001	0.30
31.709	0.0008	0.2429	1.113	0.0003	0.55
32.358	0.0012	0.3412	0.960	0.0004	0.70
31.768	0.0016	0.4267	0.800	0.0005	0.80
30.379	0.0020	0.5012	0.536	0.0008	0.90
28.507	0.0024	0.5660	0.359	0.0010	0.93
21.907	0.0036	0.7140	0.161	0.0020	0.95
14.897	0.0050	0.8243	0.073	0.0030	0.97
2.953	0.0100	0.9691	0.040	0.0050	0.99

4. Results and discussions

4.1. Static forces

A vehicle collision with bridge piers is a typical impact response, and the dynamic impact force is related to vehicular and bridge conditions such as vehicle mass, vehicle velocity, and pier structure configuration, etc. To simplify design, an equivalent static force is applied as the substitution for dynamic impact in several specifications. In Eurocode-1, the equivalent static force is regarded as a function of vehicle conditions (Suter, 2005), while a constant value of 2670 kN and 1000 kN is recommended in AASHTO-LRFD and ISPRC-DHBC, respectively.

Figure 4 presents numerical lateral force-displacement curves at the point of impact, the predicted load capacity by the present procedure and current specifications. It can be observed that at the beginning of loading, a large peak force arises corresponding to structural failure resistance. At a later stage, an approximate plateau force keeps a larger deformation relating to structural collapse, which is far smaller than its peak counterpart. For the three cases, the peak forces are far larger than 2670 kN, which means no occurrence of failure according to the AASHTO and ISPRC-DHBC standards. In addition, for Case 1, Fig. 4a shows that the simulated collapse force approximately equals the shear resistance $[F_V]$, and is less than the flexural resistance $[F_M]$, which satisfies the condition of the shear collapse mode. For Case 2, see Fig. 4b, the numerical collapse force approximates both shear and flexural resistance, conforming to flexure-shear collapse modes. For Case 3, as illustrated in Fig. 4c, the numerical collapse force as well as that in the ISPRC-DHBC standard is larger than the flexural resistance but smaller than the shear resistance, which demonstrates the flexural collapse mode. In fact, the vehicle impact on bridge piers includes a significant inertia effect, as stated by Sharma *et al.* (2009), where a large part of the impact force work transfers to structural kinetic energy.

4.2. Deformation

Figure 5 shows the deformation pattern revealing the equivalent plastic strain of pier concrete. For Case 1, an oblique shear belt can be seen between the column base and the impact point, and shear collapse occurs in accordance with the previous conclusion based on the static force analysis. For Case 2, the two deformations of oblique shear collapse and flexural collapse take place simultaneously. For Case 3, no evident shear collapse is found, while the concrete

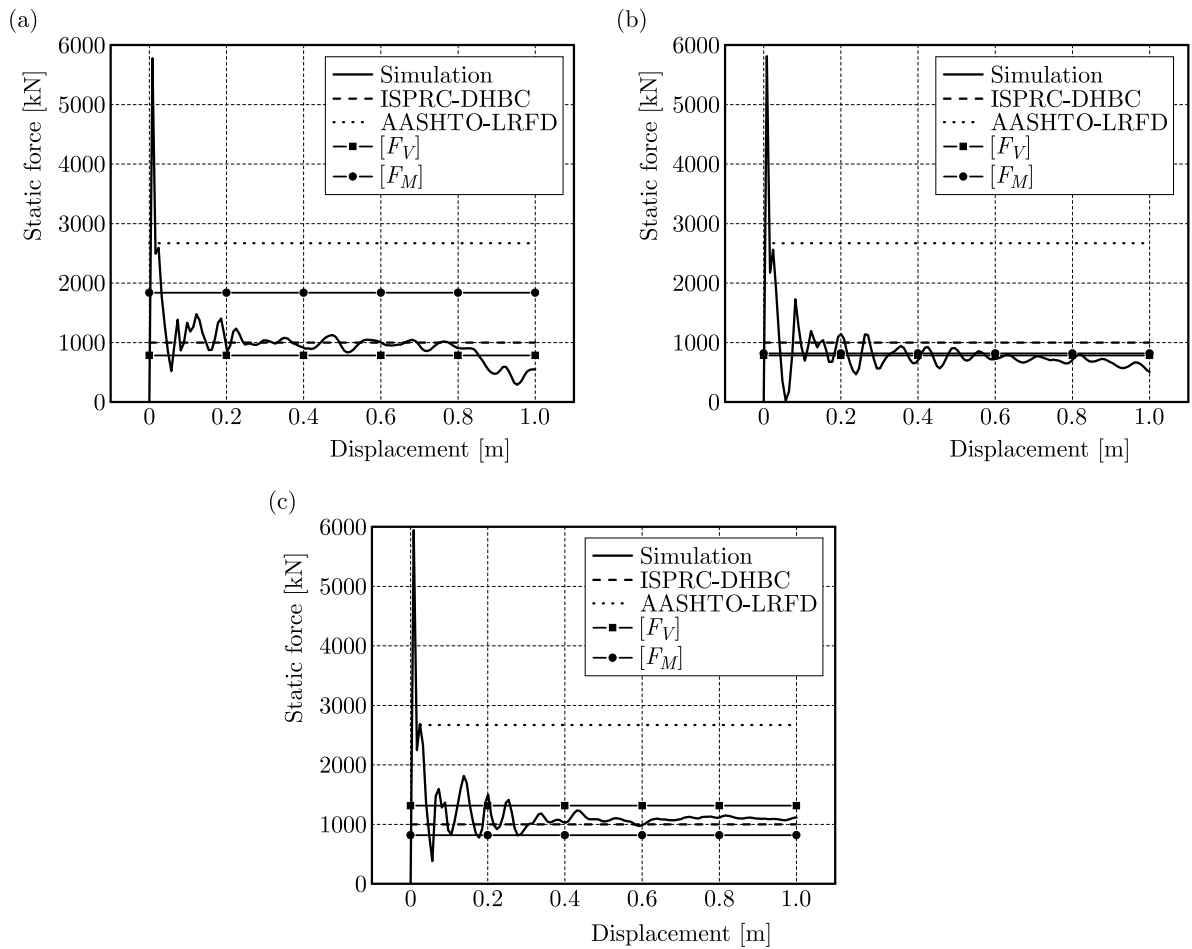


Fig. 4. Simulated lateral forces and the predicted load capacity at the loading point: (a) Case 1, (b) Case 2, (c) Case 3

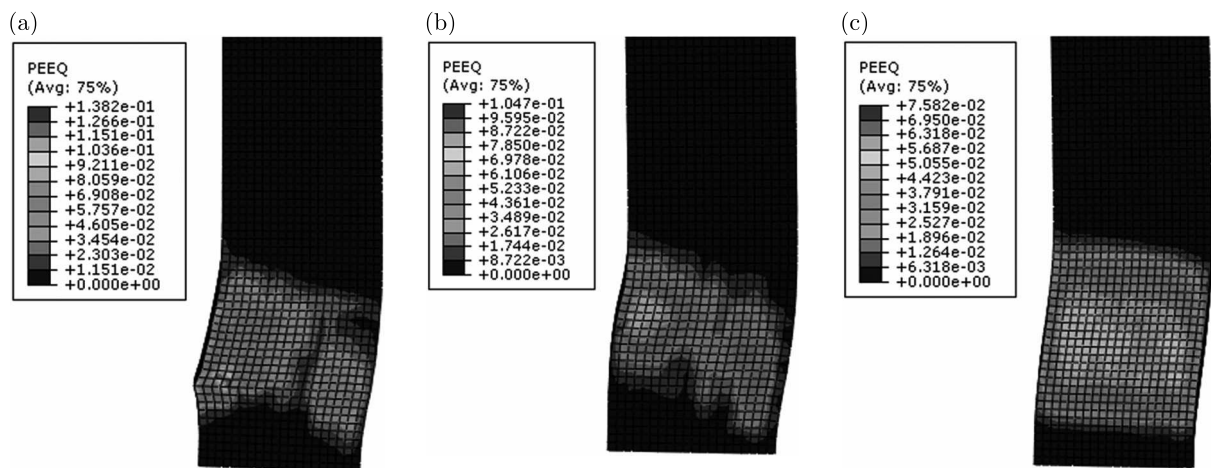


Fig. 5. Distribution of the equivalent plastic strain for pier concrete: (a) Case 1, (b) Case 2, (c) Case 3

column mainly manifests flexural deformation. In brief, for the three cases, identical conclusions are reached in terms of numerical deformation and the predicted collapse conditions, well validating the latter.

5. Conclusions

RC piers mainly experience three collapse modes, namely the shear collapse, flexural collapse and flexure-shear collapse under lateral loading. Corresponding forces for the shear and flexural collapse are obtained, where the maximum internal force comes from the simplified beam model, and the flexural resistance for the square section lies in the present model. Three cases are simulated by finite element code ABAQUS, and the deformation modes and static force analysis demonstrate almost identical conclusions. Therefore, the accuracy and adaptability of the present analytical models are well verified, which can be used for routine pier design against vehicle collision. The present framework could be useful for further investigations on other RC columns subject to transverse loading.

Acknowledgement

This research was supported by University Natural Science Research Project of Anhui Province (No. KJ2018A0481) and the Natural Science Foundation of China (No. 11972240), which are gratefully acknowledged.

References

1. ABDELKARIM O.I., ELGAWADY M.A., 2016, Performance of hollow-core FRP-concrete-steel bridge columns subjected to vehicle collision, *Engineering Structures*, **123**, 517-531
2. ABDELKARIM O., ELGAWADY M.A., 2017, Performance of bridge piers under vehicle collision, *Engineering Structures*, **140**, 337-352
3. AUYEUNG S., ALIPOUR A., SAINI D., 2019, Performance-based design of bridge piers under vehicle collision, *Engineering Structures*, **191**, 752-765
4. BUTH C.E., BRACKIN M.S., WILLIAMS W.F., FRY G.T., 2011, Collision loads on bridge piers: phase 2, *Report of Guidelines for Designing Bridge Piers and Abutments for Vehicle Collisions*, Texas Transportation Institute, Austin, TX, USA
5. CHEHAIBI K., MRAD C., NASRI R., 2019, Collision modeling of single unit impact absorber for mechanical systems vibration attenuation, *Journal of Theoretical and Applied Mechanics*, **57**, 4, 947-956
6. CHEN L., EL-TAWIL S., XIAO Y., 2016a, Reduced models for simulating collisions between trucks and bridge piers, *Journal of Bridge Engineering*, **21**, 6, 04016020
7. CHEN L., XIAO Y., EL-TAWIL S., 2016b, Impact tests of model RC columns by an equivalent truck frame, *Journal of Structural Engineering*, **142**, 5, 04016002
8. DING H., YANG Y., CHEN L.Q., YANG S.P., 2014, Vibration of vehicle-pavement coupled system based on a Timoshenko beam on a nonlinear foundation, *Journal of Sound and Vibration*, **333**, 24, 6623-6636
9. DO T.V., PHAM T.M., HAO H., 2018, Dynamic responses and failure modes of bridge columns under vehicle collision, *Engineering Structures*, **156**, 243-259
10. EL-TAWIL S., SEVERINO E., FONSECA P., 2005, Vehicle collision with bridge piers, *Journal of Bridge Engineering*, **10**, 3, 345-353
11. FUJIKAKE K., LI B., SOEUN S., 2009, Impact response of reinforced concrete beam and its analytical evaluation, *Journal of Structural Engineering*, **135**, 8, 938-950
12. GHOLIPOUR G., ZHANG C., MOUSAVI A.A., 2018, Effects of axial load on nonlinear response of RC columns subjected to lateral impact load: ship-pier collision, *Engineering Failure Analysis*, **91**, 397-418

13. HARIK I.E., SHAABAN A.M., GESUND H., VALLI G.Y.S., WANG S.T., 1990, United States bridge failures (1951-1988), *Journal of Performance of Construction Facilities*, **4**, 4, 272-277
14. HU W.P., XU M.B., SONG J.R., GAO Q., DENG Z.C., 2021, Coupling dynamic behaviors of flexible stretching hub-beam system, *Mechanical Systems and Signal Processing*, **151**, 107389
15. HU W.P., ZHANG C.Q., DENG Z.C., 2020, Vibration and elastic wave propagation in spatial flexible damping panel attached to four special springs, *Communications in Nonlinear Science and Numerical Simulation*, **84**, 105199
16. JOSHI A.S., GUPTA L.M., 2012, A simulation study on quantifying damage in bridge piers subjected to vehicle collisions, *International Journal of Advanced Structural Engineering*, **4**, 8, 1-13
17. KOSTEK R., ALEKSANDROWICZ P., 2020, Identification of the parameters of a vehicle crashing into a round pillar, *Journal of Theoretical and Applied Mechanics*, **58**, 1, 233-245
18. LIM C.W., LIEW K.M., 1994, A pb-2 Ritz formulation for flexural vibration of shallow cylindrical shells of rectangular planform, *Journal of Sound and Vibration*, **173**, 3, 343-375
19. LIM C.W., LIEW K.M., 1995, A higher order theory for vibration of shear deformable cylindrical shallow shells, *International Journal of Mechanical Sciences*, **37**, 3, 277-295
20. LIM C.W., LIEW K.M., KITIPORNCHAI S., 1998, Vibration of cantilevered laminated composite shallow conical shells, *International Journal of Solids and Structures*, **35**, 15, 1695-1707
21. SHARMA H., HURLEBAUS S., GARDONI P., 2009, A probabilistic model for the estimation of shear capacity of bridge piers subjected to dynamic loading, *Proceedings of ASCE Structures Congress*, Austin, TX, USA
22. SHARMA H., HURLEBAUS S., GARDONI P., 2012, Performance-based response evaluation of reinforced concrete columns subject to vehicle impact, *International Journal of Impact Engineering*, **43**, 52-62
23. SUTER R., 2005, Reinforcement of bridge piers with FRP sheets to resist vehicle impact, *IABSE Symposium Report*, Lisbon, Portugal
24. THILAKARATHNA H.M.I., THAMBIRATNAM D.P., DHANASEKAR M., PERERA N., 2010, Numerical simulation of axially loaded concrete columns under transverse impact and vulnerability assessment, *International Journal of Impact Engineering*, **37**, 11, 1100-1112
25. TSANG H.H., LAM N.T.K., 2008, Collapse of reinforced concrete column by vehicle impact, *Computer Aided Civil and Infrastructure Engineering*, **23**, 6, 427-436
26. WARZECHA M., MICHALCZYK J., 2020, Calculation of maximal collision force in kinematic chains based on collision force impulse, *Journal of Theoretical and Applied Mechanics*, **58**, 2, 339-349
27. YAN J.W., LAI S.K., HE L.H., 2019a, Nonlinear dynamic behavior of single-layer graphene under uniformly distributed loads, *Composites Part B*, **165**, 473-490
28. YAN J.W., TONG L.H., LUO R.J., GAO D., 2019b, Thickness of monolayer h-BN nanosheet and edge effect on free vibration behaviors, *International Journal of Mechanical Sciences*, **164**, 105163
29. YANG X.D., YANG J.H., QIAN Y.J., ZHANG W., MELNIK R.V.N., 2018, Dynamics of a beam with both axial moving and spinning motion: An example of bi-gyroscopic continua, *European Journal of Mechanics – A/Solids*, **69**, 231-237
30. ZHOU D.Y., LI R.W., WANG J., GUO C.T., 2017, Study on impact behavior and impact force of bridge pier subjected to vehicle collision, *Shock and Vibration*, **2017**, 7085392